Texture features on T2-weighted magnetic resonance imaging: New potential biomarkers for prostate cancer aggressiveness

IOP Publishing | Institute of Physics and Engineering in Medicine Physics in Medicine & Biology
Phys. Med. Biol. **00** (2015) 1–17 UNCORRECTED PROOF

Texture features on T2-weighted magnetic resonance imaging: new potential biomarkers for prostate cancer aggressiveness.

A Vignati[1], S Mazzetti[1], V Giannini[1], F Russo[1], E Bollito[2], F Porpiglia[3], M Stasi[4] and D Regge[1]

[1] Department of Radiology of Candiolo Cancer Institute—FPO, IRCCS, Strada Provinciale 142 km 3.95, 10060 Candiolo, Italy
[2] Division of Pathology of the University of Turin, San Luigi Hospital, Regione Gonzole 10, 10043 Orbassano, Italy
[3] Division of Urology and Department of Oncology of the University of Turin, San Luigi Hospital, Regione Gonzole,10, 10043 Orbassano, Italy.
[4] Department of Medical Physics of Candiolo Cancer Institute—FPO, IRCCS, Strada Provinciale 142 km 3.95, 10060 Candiolo, Italy

E-mail: vignati.anna@gmail.com

Received 17 October 2014, revised 19 January 2015
Accepted for publication 10 February 2015
Published

Abstract

To explore contrast (C) and homogeneity (H) gray-level co-occurrence matrix texture features on T2-weighted (T2w) Magnetic Resonance (MR) images and apparent diffusion coefficient (ADC) maps for predicting prostate cancer (PCa) aggressiveness, and to compare them with traditional ADC metrics for differentiating low- from intermediate/high-grade PCas.

The local Ethics Committee approved this prospective study of 93 patients (median age, 65 years), who underwent 1.5 T multiparametric endorectal MR imaging before prostatectomy. Clinically significant (volume ≥0.5 ml) peripheral tumours were outlined on histological sections, contoured on T2w and ADC images, and their pathological Gleason Score (pGS) was recorded. C, H, and traditional ADC metrics (mean, median, 10th and 25th percentile) were calculated on the largest lesion slice, and correlated with the pGS through the Spearman correlation coefficient. The area under the receiver operating characteristic curve (AUC) assessed how parameters differentiate pGS = 6 from pGS ≥ 7.

The dataset included 49 clinically significant PCas with a balanced distribution of pGS. The Spearman ρ and AUC values on ADC were: −0.489, 0.823 (mean); −0.522, 0.821 (median); −0.569, 0.854 (10th percentile); −0.556, 0.854 (25th percentile); −0.386, 0.871 (C); 0.533, 0.923 (H); while on T2w they were: −0.654, 0.945 (C); 0.645, 0.962 (H). AUC of H on ADC and T2w,

JNL:PMB PIPS: 509892 TYPE: PAP TS: NEWGEN DATE:23/2/15 EDITOR: IOP SPELLING: UK

and C on T2w were significantly higher than that of the mean ADC ($p = 0.05$).

H and C calculated on T2w images outperform ADC parameters in correlating with pGS and differentiating low- from intermediate/high-risk PCas, supporting the role of T2w MR imaging in assessing PCa biological aggressiveness.

Keywords: prostate cancer aggressiveness, pathologic Gleason score correlation, T2-weighted MR imaging, ADC maps, GLCM texture feature

AQ1 (Some figures may appear in colour only in the online journal)

1. Introduction

Prostate cancer (PCa) has traditionally been treated by whole-gland approaches, with well-known associated side-effects, such as urinary incontinence and erectile dysfunction (Potosky *et al* 2004), but also post-treatment urinary or rectal bleeding, infection in the urinary or lower gastrointestinal tract, and recto-urethral fistulae (Nam *et al* 2014, Rosenkrantz *et al* 2012). Because of the small survival benefit reported for radical prostatectomy (RP) and the generally excellent natural history reported in the series of PCa patients treated with active surveillance, there is an increasing interest in minimally invasive focal therapy or active surveillance strategies (Rosenkrantz *et al* 2012). However, current clinical paradigms used to stratify patients into risk categories, including digital rectal examination results, PSA values, and the results of transrectal ultrasound guided biopsies, among others, are affected by intrinsic errors and possible complications (Gupta *et al* 2013). As a consequence, the choice of optimal treatment strategy in some patients remains challenging. Therefore, there is a need for improved risk-stratification via noninvasive imaging in order to better identify patients who may benefit from gland-preserving strategies (Donati *et al* 2014).

Recently, efforts have been made to identify quantitative parameters derived from multiparametric Magnetic Resonance (mp-MR) imaging and to investigate their correlation with tumour aggressiveness. However, to date, robust and standardized imaging biomarkers have not yet been identified (Peng *et al* 2014, Bae *et al* 2014, Vos *et al* 2013, Kobus *et al* 2012, Vargas *et al* 2011, Turkbey *et al* 2011, Oto *et al* 2011, Hambrock *et al* 2011, Peng *et al* 2013, Jung *et al* 2013, Wang *et al* 2008). The association between apparent diffusion coefficient (ADC) values and Gleason score (GS) has been identified in both peripheral (Peng *et al* 2014, Bae *et al* 2014, Vos *et al* 2013, Kobus *et al* 2012, Vargas *et al* 2011, Turkbey *et al* 2011, Oto *et al* 2011, Hambrock *et al* 2011, Peng *et al* 2013) and transition zones (Jung *et al* 2013), but there is no consensus on the best metric to describe lesion ADC values (Donati *et al* 2014). On the other hand, the correlation of the T2 signal intensity (SI) with GS has not been uniformly observed (Wang *et al* 2008, Rosenkrantz *et al* 2010, Giannini *et al* 2014). Furthermore, the studies on T2 SI should correct SI differences across patients due to the presence of the endorectal coil (Wang *et al* 2008), introducing a potential source of errors.

The observation of correlation between pathologic GS (pGS) and lesion cellularity
AQ2 (Schiebler *et al* 1997, Quint *et al* 1991) prompted us to investigate the lesions' textural features on T2-weighted (T2w) images and ADC maps. In fact, textural features may potentially quantify texture changes due to histological alterations present in some illness (Castellano *et al* 2004). Texture, defined as a measure of spatial variations of the SI in an image, has been studied in medical image analysis to quantify image properties such as homogeneity (Chen *et al* 2007), to correlate with specific histopathologic features (Yun *et al* 2014), and to evaluate tumor heterogeneity (Herlidou-Même *et al* 2003). The texture analysis method

based on gray level co-occurrence matrix (GLCM) (Haralick *et al* 1973) has gained wide applications in medical image analysis (Chan *et al* 1995, Li *et al* 2005, Gibbs and Turnbull 2003, Freeborough and Fox 1998, Antel *et al* 2003, Mahmoud-Ghoneim *et al* 2003) for its ability to characterize the spatial dependence of gray-levels using the second-order statistics. Regarding prostate imaging, Chan *et al* (Chan *et al* 2003), Madabhushi *et al* (Madabhushi *et al* 2005), and Niaf *et al* (Niaf *et al* 2012) considered GLCM based features, in combination with other imaging parameters, to highlight PCa presence on MR images, while Viswanath *et al* (Viswanath *et al* 2012) used GLCM texture-based characterization of T2w MR data to account for spatial location of prostate disease (i.e. in the transition or peripheral zone).

However, to the best of our knowledge, GLCM texture analysis method has never been applied to differentiate PCa grade on MR imaging.

The purpose of this study was to evaluate contrast and homogeneity GLCM texture features on T2w MR images and on ADC maps as potential new biomarkers of peripheral PCa aggressiveness, and to compare them with traditional ADC metrics (mean, median, 10th and 25th percentile) (Donati *et al* 2014), to determine which parameter best differentiates low- from intermediate- or high-grade PCa lesions. The proposed strategy does not require image normalization procedures, and is, therefore, more reproducible in respect to methods based on the comparison of SI values across patients.

2. Materials and methods

The local Ethics Committee approved this prospective study and participants into the study signed informed consent forms. This study was in accordance with the Helsinki Declaration.

2.1. Patients

We enrolled prospectively 93 consecutive patients at our Institution, with the following inclusion criteria: (a) biopsy-proven adenocarcinoma, (b) mp-MR examination between April 2010 and November 2012, including axial T2w and diffusion weighted (DW) sequences, (c) RP within 3 months of MR, and (d) a clinically significant peripheral lesion (tumour volume ≥0.5 ml, Stamey *et al* 1993) at the whole-mount histopathologic analysis.

In order to build a dataset with a balanced distribution of the four pGS classes (3 + 3, 3 + 4, 4 + 3, and ≥4 + 4), a chi-squared distribution test with three degrees of freedom was applied. The idea behind the chi-square distribution test is to verify if the sample comes from the population with the claimed distribution, which is called the null hypothesis. In our study, the null hypothesis stated that the population had a balanced distribution of the four pGS classes. All available peripheral lesions with 3 + 3, 4 + 3 and ≥4 + 4 pGS were included in the dataset, while the number of pGS 3 + 4 peripheral lesions, which represent the large majority of PCa lesions (Helpap and Egevad 2006), was fixed at 14 in order to have a statistical significance higher than 0.90 to accept the null hypothesis, randomly ignoring some cases.

2.2. MR image acquisition

Images were acquired with a 1.5 T scanner (Signa Excite HD, GE Healthcare, Milwakee, Illinois, USA) using a four–channel phase-array coil combined with an endorectal coil (Medrad, Indianola, Pa). T2w images in the axial plane were obtained using the following protocol: slice-thickness, 3 mm; FOV, 16 × 16 cm; NEX, 2; acquisition matrix, 384 × 288; TR/TE ratio 3020/85. DW imaging was obtained using axial EPI sequences as follows:

slice-thickness, 3 mm, FOV 16 × 16 cm, matrix 128 × 128, NEX 6; TR/TE 7000/101; *b*-values 0 and 1000 s mm^2. Pixel-wise ADC values were calculated with in-house C++ algorithms, developed using ITK open source libraries (Johnson *et al* 2013), by using a monoexponential model (Peng *et al* 2014).

2.3. Reference standard and MR correlation

The prostate specimen was step-sectioned at 3-mm intervals perpendicular to the long axis (apical-basal) of the gland (Montironi *et al* 2001). This confidently reproduces the inclination of axial T2w images, which are acquired perpendicular to the rear gland surface. The bases and the apexes were cut parasagittally. Five μm sections were then obtained and coloured with hematoxylin eosin. The pathologist (E.B., with 24 years of experience in pathology, 20 attending uropathology) outlined each clinically significant peripheral tumour on microscopic slices and assigned a pGS.

The radiologist (F.R., with an experience of more than 500 prostate mp-MR studies interpreted per year) in consensus with the pathologist, established the reference standard for PCa on T2w images drawing freehand regions of interest (ROIs) on cancer foci, following the outlines drawn by the pathologist on digital images of the pathologic slices, annotating the whole lesion.

Always working in consensus, the radiologist and the pathologist established the locations of tumours with respect to identifiable anatomic landmarks (e.g. urethra, ejaculatory ducts, and benign prostatic hyperplasia). This imaging-pathologic correlation allowed the correct identification of tumor ROIs on T2w images and their translation from T2w images to ADC maps, even in the case of deformation of prostate specimen slices (because of the modified prostate shape soaked by formaldehyde), and deformed DW images (because of chemical shift and susceptibility artifacts).

2.4. Image analysis

The 2D GLCM texture features were calculated on the largest ROI among all the ROIs belonging to the same lesion (single-section approach) for both T2w images and ADC maps.

Each lesion ROI outlined by the radiologist was enclosed by its minimum bounding box, i.e. the smallest enclosing rectangular area of the ROI, extracted from the original image (T2w or ADC), and was saved as a new image. In the latter image, the pixel values outside the original ROI were set to the minimum intensity value of the ROI pixels in the original image (*preprocessing procedure*). This preserved the range of intensity of the original image lesion ROI. Subsequently, the GLCM was calculated on this preprocessed ROI.

The GLCM is a tabulation of how often different combinations of pixel brightness values (i.e. grey levels) occur between neighbouring pixels in an image. Therefore, the GLCM allows the calculation of *second order* texture features, i.e. describing the relationship between groups of contiguous pixels in the image (Mryka Hall-Beyer 2007).

The difference of spatial locations of two pixels in an image can be described by a displacement vector **d**. For an image of G gray levels, the $G \times G$ gray level co-occurrence matrix $P\mathbf{d}$ for a displacement vector **d** is defined as follows. The entry (i, j) of $P\mathbf{d}$ is the number of occurrences of pixel-pair of gray levels i and j whose spatial locations are a vector **d** apart. When normalized by the total counts, the entry (i, j) of $P\mathbf{d}$, denoted as $p_{i,j}$, represents the (empirical) probability of occurrence of pixel pair of gray levels i and j whose spatial locations are a vector **d** apart. In this definition, the co-occurrence matrix $P\mathbf{d}$ is a function of the

displacement vector **d**, which can be decomposed into a norm-1 distance d and a direction. Thus, $P\mathbf{d}$ describes distributions of certain spatial patterns of scale d in a certain direction (Chen *et al* 2007).

In our case, the displacement vector **d** was one pixel. Four GLCM matrices were created to describe the directions with angles 0°, 45°, 90°, and 135° with respect to the xy plane of the MR based coordinate system (Chen *et al* 2007). An additional matrix, spatially invariant, was created by averaging the counts in the four directions. In order to discard the contribution of ROI boundary pixels (which are set to the minimum gray level), the first row and the first column of the spatially invariant GLCM were removed.

Among traditional 2D GLCM features, we considered the ones measuring the contrast:

$$C = \sum_{i,j=1}^{G} p_{i,j}(i-j)^2,$$

$$H = \sum_{i,j=1}^{G} \frac{p_{i,j}}{1+(i-j)^2},$$

where C is known as contrast and H is known as homogeneity. Measures related to contrast use weights related to the distance from the GLCM diagonal. Values on the GLCM diagonal show no contrast, and contrast increases away from the diagonal. So, weights are created that increase as distance from the diagonal increases. The GLCM feature extraction and the ROI preprocessing were performed using a free software (Octave 3.8.1, GNU Octave 2014).

Four ADC metrics (mean, median, 10th and 25th percentile), identified as potentially effective in the task of classifying PCa according to the level of aggressiveness (Donati *et al* 2014), were calculated on the lesions' ROIs.

Traditional ADC metrics were calculated with a single-section approach to properly compare them with the 2D GLCM features, but the whole-lesion approach (i.e. considering the ADC histogram of all the ROIs belonging to the same lesion) was also considered, and the results of the two approaches were compared.

2.5. Statistical analysis

The relationship between image parameters and pGS was analyzed in two ways: (a) the original pGS values, divided into four categories (3 + 3, 3 + 4, 4 + 3, and ≥4 + 4), were used for Spearman correlation; (b) binary categories (pGS = 6 versus pGS ≥ 7) were used for receiver operating characteristic (ROC) analysis.

The Spearman correlation coefficient (ρ) was calculated to establish the correlation of each parameter (ADC mean, median, 10th and 25th percentile; and both ADC and T2 GLCM homogeneity and contrast) with the lesion pGS, using the method of Bland and Altman (Bland and Altman 1995) to take into account multiple lesions per patient. Besides, the Spearman correlation coefficient was calculated to characterize correlation strength between image features. Finally, the area under the ROC curve (AUC) was calculated to evaluate the ability of each image parameter to help differentiate low-risk (pGS = 6) from intermediate- or high-risk PCas (pGS ≥ 7). The 95% confidence interval of each ρ and AUC was estimated, and the AUC values of different ADC parameters were compared using the method proposed by Obuchowski (Obuchowski 1997) to take into account multiple lesions per patient.

The median and interquartile ranges were tabulated for all image parameters according to the previously reported four pGS categories. The Wilcoxon rank sum test for paired samples

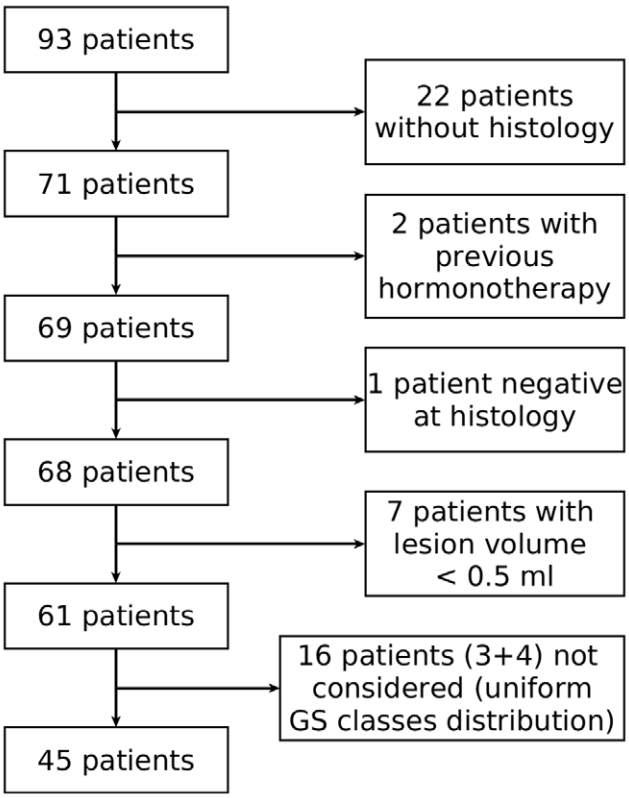

Figure 1. Flowchart of study population.

was applied to assess differences between the ADC parameters obtained with the whole-lesion and the single-section approach.

Box plots were plotted for: (a) the two best parameters, according to ρ, among all ADC parameters, and (b) the GLCM homogeneity and contrast for T2w images.

All statistical analyses were performed with MedCalc Software, version 13.2.2.0 (MedCalc Software, Ostend, Belgium), and a *p*-value of 0.05 or lower was considered statistically significant.

3. Results

From the initial cohort of 93 patients, thirty-two were excluded because of the following: the whole-mount step section pathologic tumour maps were not available ($n = 22$); received hormonal therapy at the time of MR examination ($n = 2$); did not have any confirmed cancer on the excised prostate ($n = 1$); the whole-mount histopathologic analysis did not find any clinically significant lesion in the peripheral zone of the prostate gland ($n = 7$). Flowchart in figure 1 shows the final study population.

The study population (45 patients) included 41 patients (91%) with one clinically significant tumour focus, and 4 patients (9%) with two clinically significant tumour foci, for a total of 49 clinically significant peripheral PCas. The patient and lesion characteristics are summarized in table 1.

Table 1. Patient Demographics, Clinical Characteristics, and Lesion Characteristics.

Parameter	Value
No. of patients included in study	45
Patients median age [y] (1st–3rd quartile)	65 (60–70)
Median PSA at diagnosis [ng/ml] (1st–3rd quartile)	5.9 (4.9–8.6)
Median time between MR imaging and prostatectomy [d] (1st–3rd quartile)	26 (13–47)
Median no. of days between biopsy and MR examination [d] (1st–3rd quartile)	92 (61–112)
Median prostate volume [ml] (1st–3rd quartile)	44.8 (37.3–59.5)
Clinical stage at prostatectomy[a] [no. of patients]	
T2a	9 (20%)
T2c	16 (36%)
T3a	11 (24%)
T3b	9 (20%)
No. of lesions with tumor volume ≥ 0.5 ml	49
Median volume (ml) (1st–3rd quartile)	1.6 (0.8–2.6)
Distribution of pathologic Gleason scores [no. of patients]	
3 + 3	11 (22%)
3 + 4	14 (29%)
4 + 3	13 (27%)
4 + 4	9 (18%)
4 + 5	2 (4%)

[a] Staged according to the American Joint Committee on Cancer Staging Manual, 5th edition (Fleming *et al* 1997).

Figures 2 and 3 show the pipeline to obtain ADC metrics and GLCM contrast features on two example cases, the first one referring to a low-risk PCa patient, the second referring to a high-risk PCa patient.

Table 2 shows the median values of the mean, median, 10th and 25th percentile of the ADC map according to four pGS classes (3 + 3, 3 + 4, 4 + 3, and ≥4 + 4), for both the whole-lesion and the single-section approach. No statistically significant difference was found between the two approaches. In table 2 the median values of contrast and homogeneity GLCM features are also reported according to four pGS classes for both ADC map and T2w image. Since traditional GLCM texture analysis extracts information from a 2D slice, the results of contrast and homogeneity features refer to the single-section approach. In order to facilitate the comparison of parameters, traditional ADC metrics results will hereinafter refer to the single-section approach, taking into account that the absence of statistically significant difference between the whole-lesion and the single-section approach was previously verified.

Among all ADC calculated parameters, the 10th percentile showed the highest correlation with pGS ($\rho = -0.569$), while contrast and homogeneity GLCM parameters on the T2w image showed nearly the same strong correlation with GS (respectively, $\rho = -0.654$ and 0.645) (table 3, figure 4). The correlation coefficients for all parameters were statistically significant.

The Spearman correlation coefficients between image features are reported in table 4. Traditional ADC metrics were highly correlated among them ($\rho = 0.88$–0.97), while GLCM contrast and homogeneity features (both on ADC and T2w) showed moderate/high correlation among them ($\rho = 0.64$–0.93). A moderate/low correlation was found among ADC metrics and GLCM contrast and homogeneity features, both on ADC and T2w ($\rho = 0.21$–0.50).

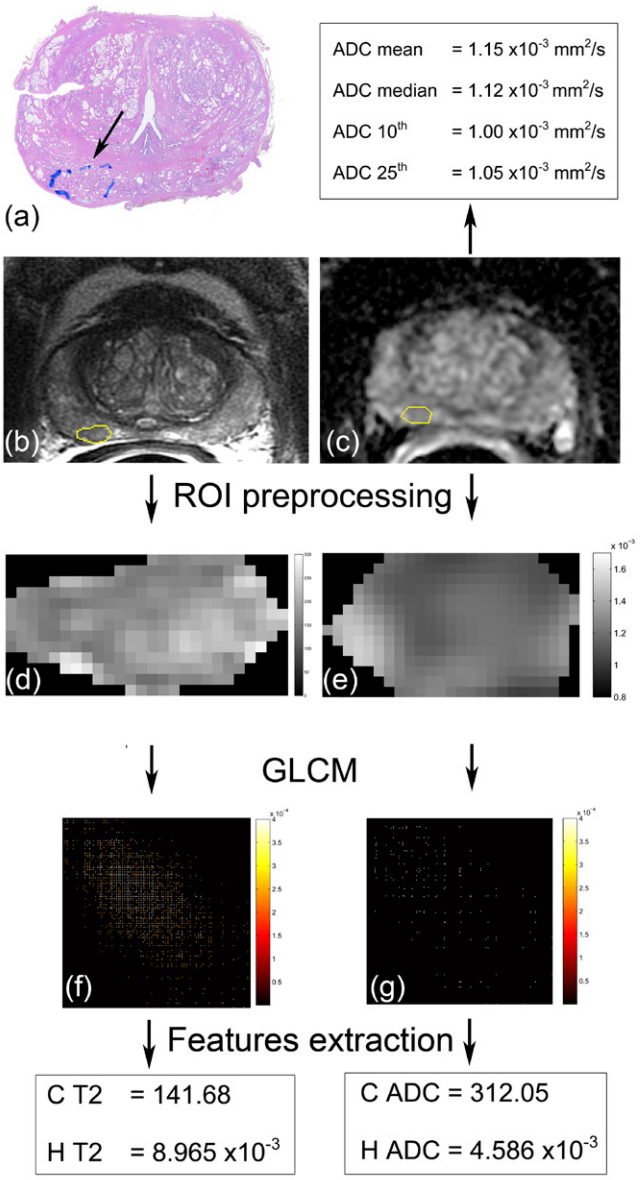

Figure 2. Method pipeline in a 64 year-old-man, with a pathology confirmed adenocarcinoma of pathologic Gleason Score 3+3 with a volume of 0.75 ml. The PCa is outlined with ink (arrow) on the histopathologic slice (*a*). Corresponding T2w image (*b*) and ADC map (*b*-values, 0 and 1000 s mm^{-2}) (*c*) show the same lesion encircled with a ROI. Traditional ADC metric values are reported. Results of the preprocessing procedure (described in the *Image Analysis* paragraph) for the T2w ROI (*d*) and the ADC ROI (*e*) are shown. GLCMs of the preprocessed T2w ROI (*f*) and the preprocessed ADC ROI (*g*) are shown. Values of contrast (C) and homogeneity (H) GLCM texture features are reported.

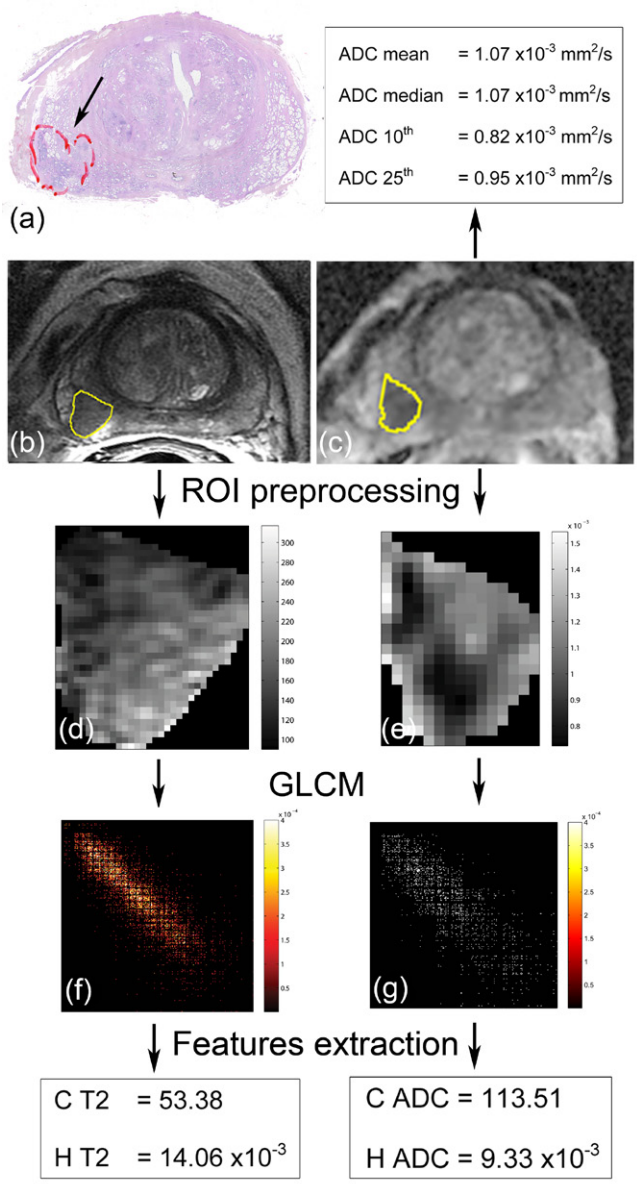

Figure 3. Method pipeline in a 61 year-old-man, with a pathology confirmed adenocarcinoma of pathologic Gleason Score 4 + 4 with a volume of 1.59 ml. The PCa is outlined with ink (arrow) on the histopathologic slice (*a*). Corresponding T2w image (*b*) and ADC map (*b*-values, 0 and 1000 s mm^{-2}) (*c*) show the same lesion encircled with a ROI. Traditional ADC metric values are reported. Results of the preprocessing procedure (described in the *Image Analysis* paragraph) for the T2w ROI (*d*) and the ADC ROI (*e*) are shown. GLCMs of the preprocessed T2w ROI (*f*) and the preprocessed ADC ROI (*g*) are shown. Values of contrast (C) and homogeneity (H) GLCM texture features are reported.

Table 2. Median values of ADC parameters, contrast and homogeneity GLCM texture features parameters.

	Pathologic gleason score	Whole-lesion approach median[a]	Single-section approach median[a]	Test whole-lesion versus single-section approach (p-value, Wilcoxon)
Mean ADC				
$\times 10^{-3}$ mm^2 s^{-1}	3 + 3	1.15 (0.94–1.26)	1.15 (0.95–1.30)	0.1475
	3 + 4	0.99 (0.87–1.10)	0.96 (0.92–1.07)	0.7148
	4 + 3	0.91 (0.83–1.10)	0.86 (0.78–1.04)	0.1909
	≥4 + 4	0.87 (0.80–0.98)	0.90 (0.80–0.96)	0.7646
Median ADC				
$\times 10^{-3}$ mm^2 s^{-1}	3 + 3	1.12 (0.94–1.31)	1.12 (0.96–1.31)	0.1230
	3 + 4	0.98 (0.85–1.09)	0.95 (0.88–1.06)	0.7609
	4 + 3	0.89 (0.80–1.08)	0.84 (0.76–1.01)	0.2734
	≥4 + 4	0.84 (0.79–0.94)	0.88 (0.79–0.94)	0.6377
10th percentile ADC				
$\times 10^{-3}$ mm^2 s^{-1}	3 + 3	0.87 (0.68–1.10)	0.90 (0.80–1.13)	0.0830
	3 + 4	0.75 (0.64–0.90)	0.75 (0.65–0.89)	0.8077
	4 + 3	0.64 (0.58–0.71)	0.64 (0.56–0.80)	0.6848
	≥4 + 4	0.65 (0.55–0.73)	0.63 (0.55–0.74)	0.4131
25th percentile ADC				
$\times 10^{-3}$ mm^2 s^{-1}	3 + 3	1.04 (0.84–1.18)	1.01 (0.88–1.22)	0.4648
	3 + 4	0.83 (0.72–0.98)	0.80 (0.75–0.97)	1.0000
	4 + 3	0.75 (0.71–0.86)	0.76 (0.68–0.89)	0.6355
	≥4 + 4	0.72 (0.65–0.82)	0.71 (0.66–0.83)	0.7002
Contrast ADC				
	3 + 3		287.4 (177.2–520.0)	
	3 + 4		148.4 (86.22–170.1)	
	4 + 3		67.43 (47.84–154.9)	
	≥4 + 4		134.2 (76.56–248.9)	
Homogeneity ADC				
$\times 10^{-3}$	3 + 3		5.239 (3.519–6.907)	
	3 + 4		8.714 (6.938–10.62)	
	4 + 3		12.09 (11.57–15.79)	
	≥4 + 4		9.334 (7.047–12.71)	
Contrast T2				
	3 + 3		150.0 (108.4–208.8)	
	3 + 4		71.99 (53.08–95.52)	
	4 + 3		46.57 (31.45–68.84)	
	≥4 + 4		41.88 (30.81–88.26)	
Homogeneity T2				
$\times 10^{-3}$	3 + 3		9.011 (7.870–9.575)	
	3 + 4		12.61 (10.93–13.52)	
	4 + 3		13.26 (12.79–15.18)	
	≥4 + 4		14.68 (10.93–15.88)	

[a] Numbers in parentheses are interquartile ranges.

Table 3. Spearman correlation coefficients for correlation of parameters with pathologic Gleason score.

	ADC		T2	
	ρ	p-value	ρ	p-value
Mean	−0.489	<0.001		
Median	−0.522	<0.001		
10th percentile	−0.569	<0.001		
25th percentile	−0.556	<0.001		
Contrast	−0.386	0.01	−0.654	<0.001
Homogeneity	0.533	<0.001	0.645	<0.001

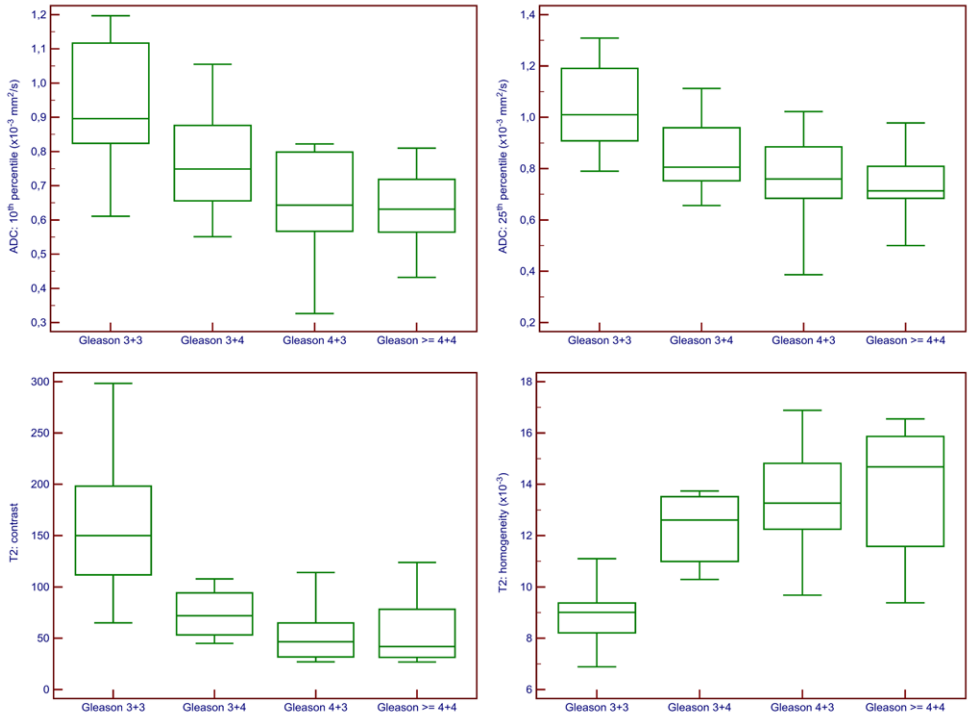

Figure 4. Box plots show comparison of 10th and 25th percentile ADC (upper line), and contrast and homogeneity GLCM texture features on T2w images (lower line) for all lesions. Line in box is median, height of box represents interquartile range, whiskers are lowest and highest data points still within 1.5 interquartile range.

In the differentiation of PCa lesions with pGS = 6 from those with pGS ≥ 7, 10th and 25th percentile ADC yielded the highest AUC (both 0.854; 95% confidence interval: 0.724, 0.939 for 10th, 0.722, 0.939 for 25th percentile) among the four ADC parameters already studied in literature. Considering all the calculated parameters, homogeneity yielded the highest AUC for both the ADC map (0.923; 95% confidence interval: 0.811, 0.980) and the T2w image (0.962; 95% confidence interval: 0.864, 0.996), followed by contrast (table 5, figure 5). The p-values for the comparison of different parameter AUC values are also reported in table 5.

Table 4. Spearman correlation coefficients (ρ) and p-values for correlation of each parameter with all the others.

		ADC						T2
ρ (p-value)		Mean	Median	10th percentile	25th percentile	Contrast	Homogeneity	Contrast
ADC	Mean	1						
	Median	0.970 (<0.0001)	1					
	10th percentile	0.884 (<0.0001)	0.895 (<0.0001)	1				
	25th percentile	0.939 (<0.0001)	0.958 (<0.0001)	0.964 (<0.0001)	1			
	Contrast	0.214 (0.1394)	0.260 (0.0709)	0.299 (0.0368)	0.318 (0.0262)	1		
	Homogeneity	−0.351 (0.0134)	−0.443 (0.0014)	−0.490 (0.0003)	−0.503 (0.0002)	−0.750 (<0.0001)	1	
T2	Contrast	0.404 (0.0040)	0.459 (0.0009)	0.495 (0.0003)	0.478 (0.0005)	0.644 (<0.0001)	−0.703 (<0.0001)	1
	Homogeneity	−0.310 (0.0304)	−0.385 (0.0062)	−0.387 (0.0061)	−0.402 (0.0042)	−0.658 (<0.0001)	0.706 (<0.0001)	−0.927 (<0.0001)

Table 5. Comparison of AUC values for differentiating tumour foci with pathologic Gleason Score 6 from those with pathologic Gleason score ≥ 7.

	AUC[a]	*p*-value	*p*-value	*p*-value	*p*-value
Mean ADC	0.823 (0.687; 0.917)	*REF*	0.886	0.325	0.064
Median ADC	0.821 (0.685; 0.915)	0.886	*REF*	0.377	0.092
10th percentile ADC	0.854 (0.724; 0.939)	0.325	0.377	*REF*	1.000
25th percentile ADC	0.854 (0.722; 0.939)	0.064	0.092	1.000	*REF*
Contrast ADC	0.871 (0.744; 0.949)	0.177	0.189	0.730	0.622
Homogeneity ADC	0.923 (0.811; 0.980)	**0.019**	**0.019**	0.206	0.067
Contrast T2	0.945 (0.840; 0.990)	**0.009**	**0.008**	0.118	**0.033**
Homogeneity T2	0.962 (0.864; 0.996)	**0.006**	**0.006**	0.073	**0.016**

[a] Numbers in parentheses are 95% confidence intervals. Each *p*-value column represents the comparison between all parameters and the reference one (*REF*). Bold values are statistically significant.

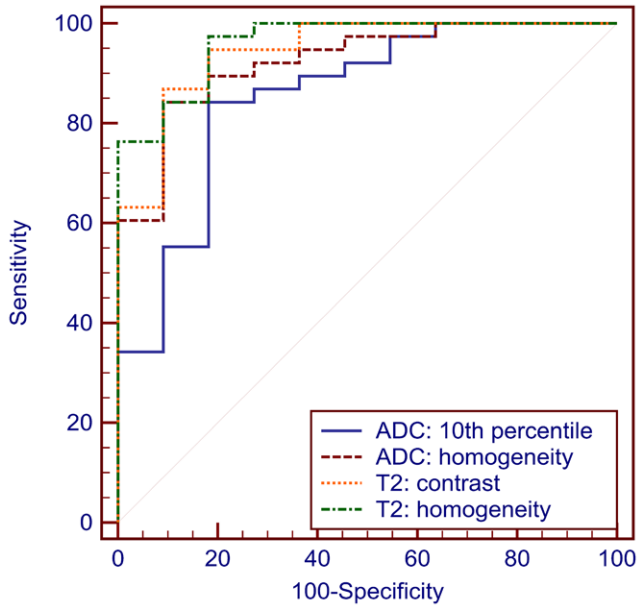

Figure 5. Comparison of ROC curves in the differentiation of tumor foci with pathologic Gleason Score of 6 from those with pathologic Gleason Score of at least 7.

4. Discussion

Investigating quantitative approaches to reliably characterize PCa aggressiveness with mp-MR imaging is a challenging task, but the stake is high. Indeed, identifying robust imaging biomarkers of PCa aggressiveness will improve patient management, opening the way to tailored treatment. While various studies demonstrate the association between ADC values and PCa aggressiveness (Vargas *et al* 2011, Turkbey *et al* 2011, Oto *et al* 2011, Hambrock *et al* 2011, Peng *et al* 2013), the correlation of the T2w images with biological tumour activity has not been clearly assessed (Wang *et al* 2008, Rosenkrantz *et al* 2010, Giannini *et al* 2014).

To evaluate the capability to non-invasively predict pGS, contrast and homogeneity GLCM texture features, calculated on both T2w MR image and ADC maps, were compared with four

ADC metrics described in the literature (mean, median, 10th and 25th percentile) (Donati *et al* 2014) in the same cohort of patients.

This study demonstrates that contrast and homogeneity GLCM texture features calculated on T2w image outperform traditional ADC parameters in correlation with pGS (ρ = −0.654, and 0.645 respectively), and yielded the highest AUC for differentiating low-risk from intermediate- or high-risk PCas compared to ADC metrics (AUC = 0.945, and 0.962 respectively). Moreover, the moderate/low correlation among ADC metrics and GLCM parameters, both on ADC and T2w, allows to hypothesize that contrast and homogeneity GLCM features may provide some additional independent information related to PCa aggressiveness.

Furthermore, a significant difference was observed between the AUC value for the homogeneity and contrast GLCM features calculated on the T2w image and the mean, median and 25th percentile of the ADC map. The AUC value for the homogeneity GLCM feature calculated on the ADC map was found significantly different from the one for the mean and median ADC parameters.

We may speculate that contrast and homogeneity GLCM texture features are affected by lesion cellularity, as well as by the presence and amount of fluid contents, collagen, and fibromuscular stroma. High-grade tumours are associated with poorly differentiated and often packed epithelial cells, while low-grade tumours have at least some individual glandular structures, which preserve some (albeit reduced) intercellular space (Peng *et al* 2014). This may explain why homogeneity (or contrast) is directly (or negatively) correlated with pGS, although large interpatient variations cause overlap in feature texture values between different pGS groups and motivate the moderate-strong correlation strength.

This study confirms that 10th and 25th percentile ADC perform better than mean and median ADC values in correlating with pGS, and in differentiating low-grade (pGS = 6) from intermediate- and high-grade tumours (pGS ≥ 7), although no significant difference was found among AUC values of traditional ADC metrics. Since a previous study stated that ADC parameters derived from whole-lesion histogram may better differentiate low-risk lesions from intermediate- and high-risk lesions (Donati *et al* 2014), we compared ADC parameters derived from the whole-lesion and the single-section approach. Contrary to Donati *et al* (Donati *et al* 2014), we did not find any statistically significant difference between the two approaches.

The range of Spearman correlation coefficients describing the relationships between ADC parameters and lesion pGS in our study (ρ = −0.489 to −0.569) lies within the previously reported values for peripheral PCas (Donati *et al* 2014, Turkbey *et al* 2011, Oto *et al* 2011, Peng *et al* 2013). AUC values for ADC parameters in discriminating low- from intermediate- and high-risk lesions (AUC = 0.821–0.854) also lie within the range of previously reported values for peripheral prostate lesions (Donati *et al* 2014, Kobus *et al* 2012, Vargas *et al* 2011, Turkbey *et al* 2011, Oto *et al* 2011, Hambrock *et al* 2011, Peng *et al* 2013). One recent study reported a higher value of AUC (0.90) for the median ADC in peripheral zone PCas (Hambrock *et al* 2011). This result may depend on the fact that the ROC analysis was calculated on only one section which included the most aggressive part of the tumour. It has been hypothesized that high tumour aggressiveness is characterized by limited intercellular space and restricted water molecule diffusion, and, thus, results in reduced ADC values. This motivates the negative correlation between ADC values and pGS, albeit large inter-patient variations cause overlap in the ADC values between high-, intermediate-, and low-grade PCa.

The strengths of this study include the use of histologic analysis performed on whole-mount sections, which is known to improve the accuracy of the MR-histologic correlation analysis of lesions (Peng *et al* 2014), and the use of a dataset characterized by uniform distribution of pGS classes (3 + 3, 3 + 4, 4 + 3, and ≥4). A balanced dataset is in fact very important

for creating a good training set, and therefore to define how accurate is a biomarker in classifying different risk classes (Mostafizur Rahman and Davis 2013).

Moreover, since GLCM textural features measure spatial variations of the SI, the proposed method does not necessitate post-processing strategies to correct differences in T2 SI ranges across patients, avoiding a related potential source of errors.

This prospective study also has limitations. First, it includes a limited number of patients and it lacks of analysis of the transition zone, because of the few PCas in this area in our cohort.

Second, the capability of GLCM features to differentiate PCa from healthy tissue, although worthy of investigation, was not explored. In fact, this study aims at investigating new potential biomarkers to predict prostate cancer aggressiveness, which represents an equally important challenge. Future research will focus on GLCM texture feature capabilities to differentiate PCa from normal-tissue, and/or PCa from benign prostatic hyperplasia or other benign abnormalities.

5. Conclusion

The results of this study suggest that, in addition to providing anatomic information, T2w endorectal MR imaging may play a primary role in assessing PCa biological aggressiveness, complementing or even improving ADC. If confirmed, this finding could positively impact on patient management. We envisage applying this new imaging marker to suspicious areas highlighted by mp-MR Computer Aided Detection (CAD) systems, providing clinicians not only with the exact location of the tumour, but allowing them also to evaluate its aggressiveness. Future studies with larger numbers of patients are warranted to confirm our results and to extend the investigation of contrast and homogeneity GLCM features for distinguishing PCa from normal tissue.

AQ3 ## Acknowledgments

This work was funded by Fondazione Piemontese per la Ricerca sul Cancro FPRC-onlus, grant Pro-Cure, 5 per Mille 2009 Ministero della Salute.

AQ4 ## References

Antel S B, Collins D L, Bernasconi N, Andermann F, Shinghal R, Kearney R E, Arnold D L and Bernasconi A 2003 Automated detection of focal cortical dysplasia lesions using computational models of their MRI characteristics and texture analysis *Neuroimage* **19** 1748–59

Bae H *et al* 2014 Apparent diffusion coefficient value as a biomarker reflecting morphological and biological features of prostate cancer *Int. Urol. Nephrol.* **46** 555–61

Bland J M and Altman D G 1995 Calculating correlation coefficients with repeated observations. II. Correlation between subjects *BMJ* **310** 633

Castellano G, Bonilha L, Li L M and Cendes F 2004 Texture analysis of medical images *Clin. Radiol.* **59** 1061–9

Chan H P, Wei D, Helvie M A, Sahiner B, Adler D D, Goodsitt M M and Petrick N 1995 Computer-aided classification of mammographic masses and normal issue: linear discriminant analysis in texture feature space *Phys. Med. Biol*. **40** 857–76

Chan I, Wells W 3rd, Mulkern R V, Haker S, Zhang J, Zou K H, Maier S E and Tempany C M 2003 Detection of prostate cancer by integration of line-scan diffusion, T2-mapping and T2-weighted magnetic resonance imaging; a multichannel statistical classifier *Med Phys*. **30** 2390–8

Chen W, Giger M L, Li H, Bick U and Newstead G M 2007 Volumetric texture analysis of breast lesions on contrast-enhanced magnetic resonance images *Magn. Reson. Med.* **58** 562–71

Donati O F, Mazaheri Y, Afaq A, Vargas H A, Zheng J, Moskowitz C S, Hricak H and Akin O 2014 Prostate cancer aggressiveness: assessment with whole-lesion histogram analysis of the apparent diffusion coefficient *Radiology* **271** 143–52

Fleming I D, Cooper J S, Henson D E, Hutter R V P, Kennedy B J, Murphy G P, O'Sullivan B, Sobin L H and Yarbro J W (ed) 1997 *American Joint Committee on Cancer Staging Manual* 5th edn (Philadelphia: Lippincott-Raven)

Freeborough PA and Fox NC 1998 MR image texture analysis applied to the diagnosis and tracking of Alzheimer's disease *IEEE Trans. Med. Imaging* **17** 475–9

Giannini V, Vignati A, Mirasole S, Mazzetti S, Russo F, Stasi M and Regge D 2014 MR-T2-weighted signal intensity: a new imaging biomarker of prostate cancer aggressiveness *Comput. Methods Biomech. Biomed. Eng.: Imag. Vis.* 1–5

Gibbs P and Turnbull L W 2003 Textural analysis of contrast-enhanced MR images of the breast *Magn. Reson. Med.* **50** 92–8

GNU Octave 2014 version 3.8.1. Available at (www.gnu.org/software/octave/)

Gupta R T, Kauffman C R, Polascik T J, Taneja S S and Rosenkrantz A B 2013 The state of prostate MRI in 2013 *Oncology* **27** 262–70

Hambrock T, Somford D M, Huisman H J, van Oort I M, Witjes J A, Hulsbergen-van de Kaa C A, Scheenen T and Barentsz J O 2011 Relationship between apparent diffusion coefficients at 3.0 T MR imaging and Gleason grade in peripheral zone prostate cancer *Radiology* **259** 453–61

Haralick R M, Sharmugam K and Dinstein I 1973 Textural features for image classification *IEEE Trans. Syst. Man Cybernet.* **3** 610–21

Helpap B and Egevad L 2006 The significance of modified Gleason grading of prostatic carcinoma in biopsy and radical prostatectomy specimens *Virchows Arch.* **449** 622–7

Herlidou-Même S, Constans J M, Carsin B, Olivie D, Eliat PA, Nadal-Desbarats L, Gondry C, Le Rumeur E, Idy-Peretti I and de Certaines J D 2003 MRI texture analysis on texture test objects, normal brain and intracranial tumors *Magn. Reson. Imag.* **21** 989–93

Johnson H J, McCormick M and Ibañez L 2013 *The ITK Software Guide* 3rd edn (Kitware) (www.itk.org/ItkSoftwareGuide.pdf)

Jung S I, Donati O F, Vargas H A, Goldman D, Hricak H and Akin O 2013 Transition zone prostate cancer: incremental value of diffusion-weighted endorectal MR imaging in tumor detection and assessment of aggressiveness *Radiology* **269** 493–503

Kobus T, Vos P C, Hambrock T, De Rooij M, Hulsbergen-Van de Kaa C A, Barentsz J O, Heerschap A and Scheenen T W 2012 Prostate cancer aggressiveness: *in vivo* assessment of MR spectroscopy and diffusion-weighted imaging at 3 T *Radiology* **265** 457–67

Li H, Giger M L, Olopade O I, Margolis A, Lan L and Chinander M R 2005 Computerized texture analysis of mammographic parenchymal patterns of digitized mammograms *Acad. Radiol.* **12** 863–73

Madabhushi A, Feldman M D, Metaxas D N, Tomaszeweski J and Chute D 2005 Automated detection of prostatic adenocarcinoma from high-resolution *ex vivo* MRI *IEEE Trans. Med. Imaging* **24** 1611–25

Mahmoud-Ghoneim D, Toussaint G, Constans J M and de Certaines J D 2003 3D texture analysis in MRI: a preliminary evaluation in gliomas *Magn. Reson. Imag.* **21** 983–7

Montironi R, Lopez-Beltran A, Mazzucchelli R, Scarpelli M and Bollito E 2001 Assessment of radical prostatectomy specimens and diagnostic reporting of pathological findings *Pathologica* **93** 226–32

Mostafizur Rahman M and Davis D N 2013 Addressing the class imbalance problem in medical datasets *Int. J. Mach. Learn. Comput.* **3** 224–8

Hall-Beyer M 2007 The GLCM tutorial home page, available at: www.fp.ucalgary.ca/mhallbey/tutorial.htm. Accessed 16 June 2014

Nam R K *et al* 2014 Incidence of complications other than urinary incontinence or erectile dysfunction after radical prostatectomy or radiotherapy for prostate cancer: a population-based cohort study *Lancet. Oncol.* **15** 223–31

Niaf E, Rouvière O, Mège-Lechevallier F, Bratan F and Lartizien C 2012 Computer-aided diagnosis of prostate cancer in the peripheral zone using multiparametric MRI *Phys. Med. Biol.* **57** 3833–51

Obuchowski N A 1997 Nonparametric analysis of clustered ROC curve data *Biometrics* **53** 567–78

Oto A, Yang C, Kayhan A, Tretiakova M, Antic T, Schmid-Tannwald C, Eggener S, Karczmar G S and Stadler W M 2011 Diffusion-weighted and dynamic contrast-enhanced MRI of prostate cancer:

correlation of quantitative MR parameters with Gleason score and tumor angiogenesis *AJR Am. J. Roentgenol.* **197** 1382–90

Peng Y, Jiang Y, Antic T, Giger M L, Eggener S E and Oto A 2014 Validation of quantitative analysis of multiparametric prostate MR images for prostate cancer detection and aggressiveness assessment: a cross-imager study *Radiology* **271** 461–71

Peng Y, Jiang Y, Yang C, Brown J B, Antic T, Sethi I, Schmid-Tannwald C, Giger M L, Eggener S E and Oto A 2013 Quantitative analysis of multiparametric prostate MR images: differentiation between prostate cancer and normal tissue and correlation with Gleason score—a computer-aided diagnosis development study *Radiology* **267** 787–96

Potosky A L, Davis W W, Hoffman R M, Stanford J L, Stephenson R A, Penson D F and Harlan L C 2004 Five-year outcomes after prostatectomy or radiotherapy for prostate cancer: the prostate cancer outcomes study *J. Natl Cancer Inst.* **96** 1358–67

Quint L E, Van Erp J S, Bland P H, Del Buono E A, Mandell S H, Grossman H B and Gikas P W 1991 Prostate cancer: correlation of MR images with tissue optical density at pathologic examination *Radiology* **179** 837–42

Rosenkrantz A B *et al* 2012 Prostate cancer: multiparametric MRI for index lesion localization—a multiple-reader study *AJR Am. J. Roentgenol.* **199** 830–7

Rosenkrantz A B, Kopec M, Kong X, Melamed J, Dakwar G, Babb J S and Taouli B 2010 Prostate cancer versus post-biopsy hemorrhage: diagnosis with T2- and diffusion-weighted imaging *J. Magn. Reson. Imag.* **31** 1387–94

Schiebler M L, McSherry S, Keefe B, Mittelstaedt C A, Mohler J L, Dent G A and McCartney W H 1991 Comparison of the digital rectal examination, endorectal ultrasound, and body coil magnetic resonance imaging in the staging of adenocarcinoma of the prostate *Urol. Radiol.* **13** 110–18 AQ8

Stamey T A, Freiha F S, McNeal J E, Redwine E A, Whittemore A S and Schmid H P 1993 Localized prostate cancer. Relationship of volume to clinical significance for treatment of prostate cancer *Cancer* **71** 933–8

Turkbey B *et al* 2011 Is apparent diffusion coefficient associated with clinical risk scores for prostate cancers that are visible on 3 T MR images? *Radiology* **258** 488–95

Vargas H A, Akin O, Franiel T, Mazaheri Y, Zheng J, Moskowitz C, Udo K, Eastham J and Hricak H 2011 Diffusion-weighted endorectal MR imaging at 3 T for prostate cancer: tumor detection and assessment of aggressiveness *Radiology* **259** 775–84

Viswanath S E, Bloch N B, Chappelow J C, Toth R, Rofsky N M, Genega E M, Lenkinski R E and Madabhushi A 2012 Central gland and peripheral zone prostate tumors have significantly different quantitative imaging signatures on 3 T endorectal, *in vivo* T2-weighted MR imagery *J. Magn. Reson. Imag.* **36** 213–24

Vos E K, Litjens G J, Kobus T, Hambrock T, Hulsbergen-van de Kaa C A, Barentsz J O, Huisman H J and Scheenen T W 2013 Assessment of prostate cancer aggressiveness using dynamic contrast-enhanced magnetic resonance imaging at 3 T *Eur. Urol.* **64** 448–55

Wang L, Mazaheri Y, Zhang J, Ishill N M, Kuroiwa K and Hricak H 2008 Assessment of biologic aggressiveness of prostate cancer: correlation of MR signal intensity with Gleason grade after radical prostatectomy *Radiology* **246** 168–76

Yun B L, Cho N, Li M, Jang M H, Park S Y, Kang H C, Kim B, Song I C and Moon W K 2014 Intratumoral heterogeneity of breast cancer Xenograft models: texture analysis of diffusion-weighted MR imaging *Korean J. Radiol.* **15** 591–604

QUERIES

Page 2
AQ1
Please be aware that the colour figures in this article will only appear in colour in the web version. If you require colour in the printed journal and have not previously arranged it, please contact the Production Editor now.
AQ2
Reference Schiebler et al (1997) is cited in text but not provided in the list. Please provide complete publication details to insert in the list, else delete the citation from the text.
Page 15
AQ3
We have been provided funding information for this article as below. Please confirm whether this information is correct.
“Fondazione Piemontese per la Ricerca sul Cancro FPRC-onlus:grant Pro-Cure”.
AQ4
Please check the details for any journal references that do not have a link as they may contain some incorrect information.
Page 16
AQ5
Please provide the volume for Giannini et al (2014).
AQ6
Please update the publication details if appropriate in GNU Octave (2014).
AQ7
Please provide the publisher location for Johnson et al (2013).
Page 17
AQ8
Reference Schiebler et al (1991) is listed in the reference list but not cited in the text. Please cite in the text, else delete from the list.